Check for updates

Small

NANO · MICRO small
www.small-journal.com

RESEARCH ARTICLE OPEN ACCESS

Quantitative Imaging of Human Hemoglobin Binding to *Staphylococcus aureus* With Single-Molecule Resolution

Pietro Delcanale[1] | Andrea Mussini[1] | Òscar Gulías[2] | Montserrat Agut[2] | Melissa Berni[3] | Stefano Pongolini[3] | Stefano Bruno[4] | Alessandro Casnati[5] | Santi Nonell[2,6] | Cristiano Viappiani[1] | Stefania Abbruzzetti[1]

[1]Dipartimento Di Scienze Matematiche, Fisiche e Informatiche, Università di Parma, Parma, Italy | [2]Institut Químic de Sarrià, Universitat Ramon Llull, Barcelona, Spain | [3]Risk Analysis and Genomic Epidemiology Unit, Istituto Zooprofilattico Sperimentale Della Lombardia e dell'emilia-Romagna, Parma, Italy | [4]Dipartimento Di Scienze degli Alimenti e del Farmaco, Università di Parma, Parma, Italy | [5]Dipartimento Di Scienze Chimiche, della Vita e della Sostenibilità Ambientale, Università di Parma, Parma, Italy | [6]Catalan Institution for Research & Advanced Studies, ICREA, Barcelona, Spain

Correspondence: Pietro Delcanale (stefania.abbruzzetti@unipr.it) | Stefania Abbruzzetti (stefania.abbruzzetti@unipr.it)

Received: 1 January 2026 | **Revised:** 3 August 2026 | **Accepted:** 6 August 2026

Keywords: d-STORM | iron-regulated surface determinant | photodynamic therapy | Staphylococcus aureus | super resolution microscopy

ABSTRACT

Staphylococcus aureus is a widespread human pathogenic bacterium that poses an increasingly serious threat to public health worldwide, due to the emergence and spread of antibiotic-resistant strains. A key virulence mechanism is the acquisition of iron from the heme group of human host's hemoglobin, initiated by hemoglobin binding to receptors exposed on the bacterial surface. Although this interaction is a promising target for new antimicrobials, quantitative data on hemoglobin capture by single bacteria are lacking. In this work, single-molecule localization microscopy is used to directly quantify the number of hemoglobin molecules captured by individual *S. aureus* cells and resolve their nanoscale spatial distribution at the sub-cellular level. This quantitative approach provides a methodological framework to monitor, with single-molecule sensitivity, changes in surface density of functional receptors in response to iron limitations. This piece of information, in turn, is critical to define the overall efficacy of antimicrobials targeting bacterial receptors. As proof of this concept, we develop a photo-activated molecular system based on hemoglobin for targeted photodynamic inactivation of *S. aureus*.

1 | Introduction

Staphylococcus aureus is a commensal microorganism, commonly found on the skin and in the nasal cavities of humans. This bacterium can become a dangerous human pathogen, usually following lesions of skin or mucosal barrier. One of the main challenges in the clinical treatment of *S. aureus* infections is the emergence and spread of antibiotic-resistant strains [1]. Antibiotic resistance represents a major global threat, because it reduces the efficacy of standard antibiotics and exposes humanity to serious risks. The urgency of this issue is demonstrated by reports of WHO predicting that antibiotic resistance could cause up to 39 million deaths by 2050, also due to a scarcity of new drugs and a lack of innovative methods against resistant bacteria [2]. In this context, methicillin-resistant *S. aureus* is one of the major concerns. Therefore, developing novel and alternative methods specifically directed against *S. aureus* is particularly urgent.

Since *S. aureus* must acquire iron ions (Fe) from the human host to proliferate, molecular systems involved in Fe acquisition are regarded as potential therapeutic targets, alternative or complementary to existing antibiotics. *S. aureus* can acquire extracellular Fe, for instance from the human Fe-binding proteins transferrin and lactoferrin, through the secretion of siderophores.

This is an open access article under the terms of the Creative Commons Attribution License, which permits use, distribution and reproduction in any medium, provided the original work is properly cited.
© 2026 The Author(s). *Small* Functional Materials published by Wiley-VCH GmbH

Siderophores are small molecules that bind Fe with extremely high affinity and are subsequently recognized by specific bacterial receptors [3, 4]. Upon red blood cell lysis by secreted hemolysins, *S. aureus* can also acquire Fe from the heme cofactor in human hemoglobin (Hb). This process is mediated by bacterial Fe-regulated surface determinant (Isd) proteins that bind Hb, extract the heme, and transport it into the cytoplasm for degradation and Fe release [5]. The role of the Isd system is crucial as heme is considered the preferred Fe source in early *S. aureus* infections and, additionally, mutants lacking Isd proteins show reduced virulence [6, 7].

The binding of Hb to the surface of *S. aureus* occurs on two receptors of the Isd system: IsdB and IsdH. If the predominant role of IsdB in binding free Hb is well established, the contribution of IsdH is still under consideration. In fact, IsdH has been demonstrated to bind in vivo the complex between Hb and haptoglobin and possibly Hb at low concentration and to be very important in determining survival of *S. aureus* to phagocytosis in human blood [8]. Interestingly, very recently Bettati and coworkers have reported the structural analysis of Hb binding to full-length IsdH [9], but experiments in vivo are still missing. Upon binding, IsdB and IsdH extract the heme from Hb and pass it to another surface-exposed protein (IsdA) or to other downstream Isd proteins for further transport [4].

Because IsdB, IsdH and IsdA proteins are exposed on the bacterial surface, they constitute potential accessible targets for antimicrobials. Small molecules designed to inhibit the interaction between IsdB and Hb have been proposed as an alternative class of antibiotics [10]. Monoclonal antibodies directed to IsdA and IsdB showed protection against *S. aureus* infection in murine models [11, 12]. Nanobodies obtained from camelid immunoglobulins targeting IsdH and IsdB have been shown to block heme acquisition and inhibit bacterial growth [13]. Monoclonal antibodies targeting IsdB and IsdA, conjugated with the photosensitizing molecule IRDye 700DX, and combined with a second intracellular photosensitizer, have been used for effective light-activated elimination of *S. aureus* [14].

As IsdB and IsdH are the predominant Hb receptors, the structure of their complex with Hb, as well as the dynamics underlying heme transfer from Hb to bacterial Isd proteins, have been extensively studied [9, 15, 17] In contrast, much less is known about the number and sub-cellular distribution of Hb molecules that are effectively captured on the bacterial surface, which is crucial in the overall Fe acquisition process. In a previous study, fluorescence microscopy indicated a strong change of IsdB signal in response to the amount of Fe available during bacterial growth and demonstrated the co-localization of IsdB and IsdA at discrete locations on the cell surface [18]. These results highlighted the importance of visualizing proteins at sub-cellular level, yet they were unable to provide a quantitative picture of the capture of Hb on the cell surface.

In this work, we use a single-molecule fluorescence imaging methodology, based on direct stochastic optical reconstruction microscopy (d-STORM) [19], to quantify the number and nanoscale distributions of Hb proteins bound on the surface of *S. aureus*. Because the binding of Hb proteins is the first event in the Fe acquisition process mediated by the Isd system, an absolute quantification of these proteins at the level of single cell and single molecule is expected to support the design of future antimicrobial strategies, complementing structural information and biological assays.

We estimate that a single *S. aureus* cell can bind, on average, ~450 Hb molecules under Fe starving conditions. We also show that proteins are organized in clusters on *S. aureus* cells. Finally, in a proof-of-principle application, we show that the efficacy of light-activated microbial inactivation by methylene blue labelled Hb, is related to the absolute number of Hb copies bound on the bacteria. The results pave the way to a rational development of antimicrobials acting on the Isd system.

2 | Results and Discussion

2.1 | Sub-Diffraction Visualization of Hb on S. Aureus Cells

In a first fluorescence imaging experiment, *S. aureus* was grown until reaching the stationary phase under Fe starving conditions by adding 1 mM of the Fe chelator 2,2-dipyridyl (DiP) to the culture medium. The reduced Fe availability is known to increase the expression of Hb receptors, which in turns increases the amount of Hb molecules captured on the cell surface [18]. After chemical fixation, bacteria were incubated with 4 μM of Hb conjugated with the AlexaFluor647 fluorophore (Hb-AF647) and with the wheat germ agglutinin—AlexaFluor488 conjugate (WGA-AF488), which labels the cell wall of Gram-positive bacteria and was used as a reference. Figure 1a illustrates a cartoon representing the labeling results, where Hb-AF647 targets the available receptor proteins and WGA-AF488 locates on the cell wall of *S. aureus*.

It is worth mentioning that, at the employed concentration, Hb retains its tetrameric structure (with two dimers, $\alpha_1\beta_1$ and $\alpha_2\beta_2$, composed of α and β subunits), as oxy-Hb dissociates into dimers with characteristic dissociation constants in the sub-micromolar range at neutral pH [20, 21]. Even if *S. aureus* can acquire Fe from Hb at 10–100 nM concentrations [7], recent cryo-EM studies demonstrated that the first events of the heme extraction process involve the interaction of IsdB with tetrameric Hb [16].

Since Hb-AF647 and WGA-AF488 emit in spectrally separated detection channels, two-color d-STORM imaging was performed to simultaneously localize these species with sub-diffraction precision. The acquired d-STORM images (Figure 1b) show that Hb-AF647 fluorescence (red) colocalizes with that of WGA-AF488 (green) on the surface of the *S. aureus* cells, ensuring that the observed Hb molecules are bound to the bacterial surface. Additionally, the sub-cellular spatial distribution of the fluorescent molecules on *S. aureus* was resolved at the nanoscale. WGA-AF488 (green) labels the cell wall of bacteria, even if with some inhomogeneities, generating typical ring-like fluorescence patterns of ~800 nm diameter, occurring when bacteria are in the focal plane of the microscope. This signal serves as reference to easily identify individual cells, even within groups of adjacent bacteria. The fluorescence of Hb-AF647 (red) was also clearly located on the cell surface, but in a discontinuous way, characterized by clusters and point-like structures, reflecting

16136829, 0, Downloaded from https://onlinelibrary.wiley.com/doi/10.1002/smll.75276 by CochraneItalia, Wiley Online Library on [18/08/2026]. See the Terms and Conditions (https://onlinelibrary.wiley.com/terms-and-conditions) on Wiley Online Library for rules of use; OA articles are governed by the applicable Creative Commons License

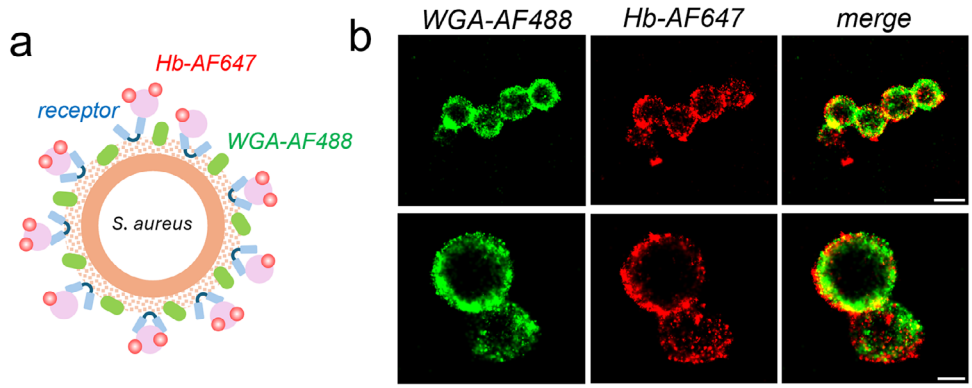


FIGURE 1 | Sub-diffraction visualization of Hb on *S. aureus* cells. (a) Cartoon representing the fluorescent labeling of *S. aureus* cells used for d-STORM imaging: Hb-AF647 binds to available receptors and WGA-AF488 stains the cell wall. (b) Representative d-STORM images of *S. aureus* where the reference WGA-AF488 (green, left) and Hb-AF647 (red, middle) channels are separately shown, together with the corresponding two-color image (right). Scale bars: 1 μm (top) and 500 nm (bottom).

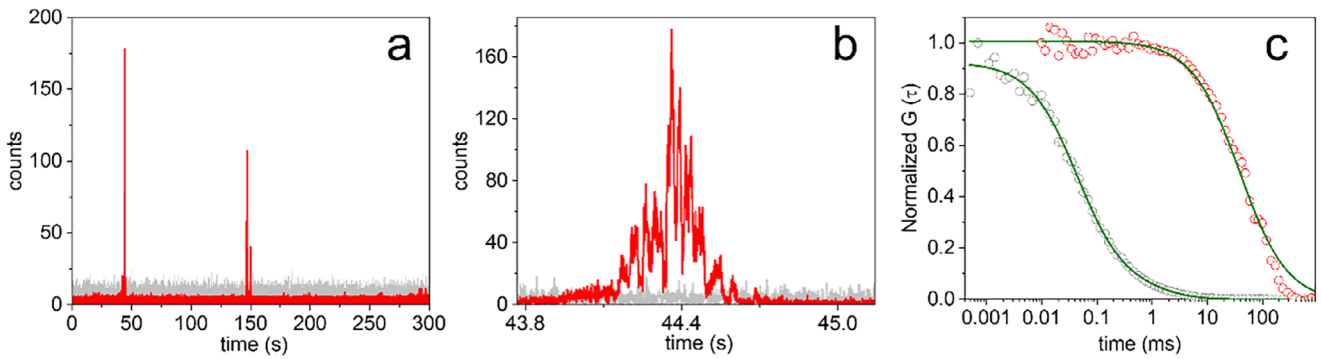


FIGURE 2 | Binding of Hb to *S. aureus* through Fluorescence Correlation Spectroscopy. (a) Photon count traces for Hb-AF647 in PBS (1 nM, gray trace) and for Hb-AF647 (1 nM) exposed to *S. aureus* (OD at 600 nm = 0.3, red trace). Photon binning is 1 ms. Excitation at 635 nm, detection at 675/25 nm. Bacteria were grown in the presence of 0.25 mM DiP. (b) Zoom of a selected portion of the photon count traces shown in panel (a). (c) Normalized autocorrelation functions computed on signals in panel (a) on a 5 min time acquisition. The green lines are the result of a fitting with a model comprising a triplet state and one diffusing species.

a non-homogeneous capture of Hb molecules on the surface (Figure 1b). A qualitatively similar Hb organization was also reported by Physchany et al. [18]., but with significantly lower resolution and sensitivity.

2.2 | Fluorescence Correlation Spectroscopy Shows Binding of Hb to S. Aureus

To further confirm binding of Hb-AF647 to bacteria, we performed Fluorescence Correlation Spectroscopy (FCS) measurements. This technique can detect interactions of dye-labeled proteins with bulkier species, including bacteria, with high sensitivity. Compared to fluorescence imaging, FCS operates on species that diffuse in a homogeneous solution and does not require multi-step protocols of staining and surface immobilization of bacteria. In this way, the binding observed with d-STORM imaging could be validated using a different experimental approach, even if FCS cannot provide the spatial distribution of molecules.

During the acquisition time, FCS monitors fluorescence originating from a fixed point in the solution, corresponding to the small (~10^{-15} L) detection volume of a confocal microscope. The fluorescence intensity time-traces in Figure 2a demonstrate that when Hb-AF647 is exposed to *S. aureus* (red), some high spikes appear, due to the diffusion of bacteria-bound Hb-AF647 through the confocal volume of the microscope, in comparison with the fluorescence fluctuations observed with only Hb-AF647 in solution (gray). The high intensity of the spikes shows that several copies of the dye are decorating the surface of a cell (Figure 2b). The associated correlation curves (Figure 2c) support this hypothesis, showing a clear increase in the diffusion time in the presence of *S. aureus* (red curve) in comparison with the value for Hb-AF647 alone (gray curve).

In particular, the correlation curve for Hb-AF647 is best described by a single diffusing species with a diffusion time τ_D = 0.29 ± 0.01 ms and an additional kinetic phase with much shorter lifetime, τ_T = 72 ± 2 μs, which is due to the formation of dark states of the AF647 dye. It is worth noting that the measured τ_D is somewhat shorter than expected, considering the size and molecular weight of tetrameric Hb. The single molecule level in FCS experiments forces us to use very low concentrations of the protein complex (1 nM). This entails that Hb does not retain its full tetrameric form, tending to dissociate mainly to dimers and possibly monomers, albeit their presence has been reported only

16136829, 0, Downloaded from https://onlinelibrary.wiley.com/doi/10.1002/smll.75276 by CochraneItalia, Wiley Online Library on [18/08/2026]. See the Terms and Conditions (https://onlinelibrary.wiley.com/terms-and-conditions) on Wiley Online Library for rules of use; OA articles are governed by the applicable Creative Commons License

at acidic and alkaline conditions [22]. Moreover, we cannot rule out the possibility that the S/N ratio doesn't allow for a precise separation between the photophysics of the fluorophore (dark states of AF647) and the diffusive process. However, it is clear that in presence of *S. aureus*, the dyes diffuse more slowly (τ_D = 38 ± 1 ms) this is evidence of Hb-AF647 molecules diffusing in solution attached to bacteria. Moreover, assuming a spherical model, a diffusion coefficient D = 0.56 μm^2/s is estimated, from which the hydrodynamic radius of the bacterium can be obtained, R_h ~ 430 nm, through the Stokes-Einstein equation. This value is in line with the expected dimension of *S. aureus* cells [23, 24].

2.3 | Distribution of Hb on single S. aureus cells

We then investigated the amount of surface bound Hb per bacterium. This is relevant as the ability of *S. aureus* to acquire Fe from Hb can change significantly in response to mutated external conditions such as availability of Fe in solution, which is a major parameter determining the expression of Isd proteins [18].

We therefore grew *S. aureus* in culture medium enriched with different concentrations of the Fe chelating agent DiP, from 0 to 1 mM, to modulate the expression of Hb receptors. As described above, we exposed the cells, in the stationary phase, to 4 μM of Hb-AF647, performed the reference staining of the cell wall with WGA-AF488, and finally acquired two-color d-STORM images. Representative examples of acquired images are shown in Figure 3a, where Hb-AF647 fluorescence is in red and the reference WGA-AF488 fluorescence is in green.

It can be readily appreciated that the amount of surface bound Hb increases with increasing concentration of the Fe chelator DiP in the growth medium. Moreover, in all tested conditions, the spatial organization of Hb on the cell surface is highly non-homogeneous. Notably, a few red spots per cell (Figure 3a), which correspond to single or small clusters of Hb molecules captured on the bacterial surface, were observed in bacteria grown in absence of DiP. This signal is low but clearly higher than negative control samples (see next section and Figure S1). Such low surface density of Hb could not have been observed with traditional microscopy [18]. We also point out that, in d-STORM images, Hb molecules are directly detected through the chemical conjugation with small AF647 dyes, avoiding the introduction of additional exogenous probes, e.g., bulky antibodies, which might introduce labeling errors at single-molecule level.

These observations highlight a superior sensitivity of the method which enables the detection of very low protein levels, as already demonstrated for target receptors exposed on cancer cells [25, 26].

In d-STORM imaging, each fluorophore undergoes blinking (on/off switching) during a time-course acquisition with continuous laser excitation. When a single fluorophore transiently turns on during acquisition, its center position, called localization, is determined with sub-diffraction precision (~20 nm [19]) so that the final image is reconstructed by merging all the localizations. The number of localizations generated by Hb-AF647 is therefore proportional to the actual number of proteins and it was used as a semi-quantitative parameter to evaluate the amount of Hb per bacterium. To do so, we first manually selected circular

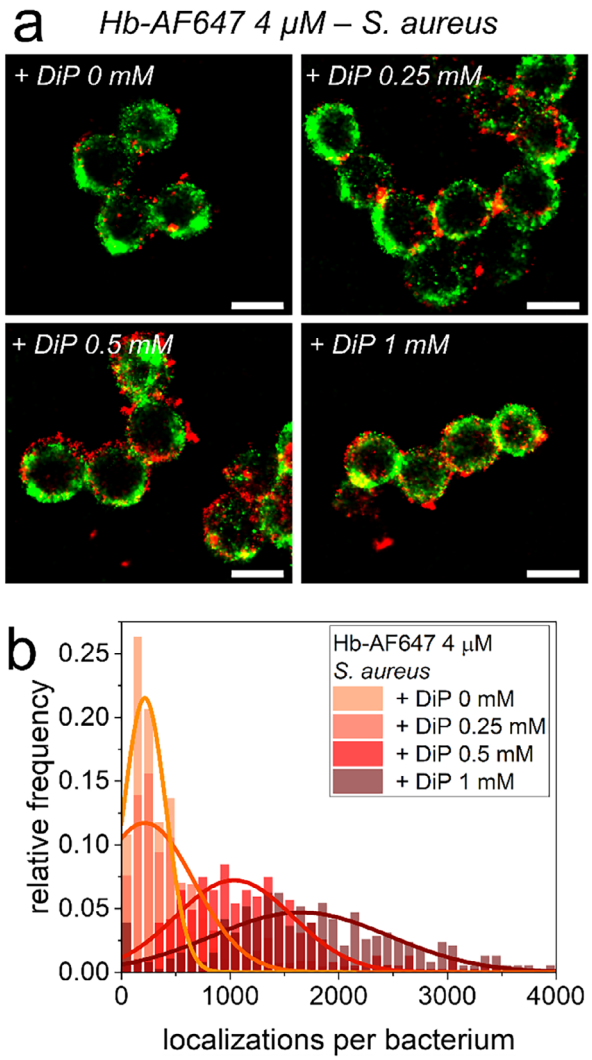


FIGURE 3 | Distributions of counted localizations per bacterium for *S. aureus* grown at different concentrations of DiP. (a) Representative two-color d-STORM images of *S. aureus* exposed to Hb-AF647 (red) and stained with WGA-AF488 (green), obtained for bacteria grown in medium supplemented with increasing concentration of DiP. Scale bars: 1 μm. (b) Distributions of the counted localizations per bacterium, in the AF647 channel, obtained from d-STORM images of bacteria grown in medium supplemented with 0 (N = 315), 0.25 (N = 712), 0.5 (N = 389) and 1 mM (N = 386) DiP concentrations. The continuous lines show the results of the fitting with a Gaussian model.

areas comprising single *S. aureus* in the d-STORM images. This selection was done on the WGA-AF488 reference signal (green) to include bacteria that are well focused and show the typical ring-like pattern. Then, the number of Hb-AF647 localizations (red) within each selected area was counted (see Figure S2 for an example). The results of the analysis are in Figure 3b, which shows the distributions of counted localizations per bacterium for *S. aureus* grown at different concentrations of DiP. The fitting with a Gaussian model clearly highlights changes in the observed distributions. In absence of DiP, the distribution is sharply peaked around relatively small values of localizations per cell (peak = 216, width = 316). At 0.25 mM DiP, the distribution remains peaked at 216 localizations per bacterium, but it is broadened (width = 911), with a tail extending to larger values. This reflects the

16136829, 0, Downloaded from https://onlinelibrary.wiley.com/doi/10.1002/smll.75276 by CochraneItalia, Wiley Online Library on [18/08/2026]. See the Terms and Conditions (https://onlinelibrary.wiley.com/terms-and-conditions) on Wiley Online Library for rules of use; OA articles are governed by the applicable Creative Commons License

presence of more Hb bound per bacterium and, more specifically, the appearance of larger Hb clusters on bacteria (Figure 3a). At higher DiP concentrations (0.5 and 1 mM), the observed distributions shift to larger peak values (peak = 1036 and 1650, for 0.5 mM and 1 mM DiP, respectively) and, at the same time, become broader and less defined (width = 1078 and 1630, for 0.5 mM and 1 mM DiP, respectively). This analysis confirms that the amount of captured Hb strongly increases for bacteria that are exposed to a reduced concentration of Fe in solution. It also demonstrates that the amount of Hb loaded on single bacterial cells is extremely variable, especially under Fe starving conditions. A marked heterogeneity was also observed for the spatial organization of Hb molecules on the bacterial surface, that always showed discontinuities, clusters and patches, far from a homogeneous covering.

2.4 | Hb Copies on Single *S. aureus* Cells

The previous semi-quantitative analysis relies on the fact that the localization counts are roughly proportional to the number of fluorescent molecules. However, retrieving the actual number of Hb-AF647 copies from the localization counts is not obvious, as a single fluorophore typically generates multiple localizations during acquisition, with an intrinsic variability, and, additionally, the dye-protein stoichiometry is also variable. Many methods have been proposed for accurate molecule counting [27]. For these data, we used a simplified approach to estimate the number of surface bound Hb-AF647. Briefly, a calibration was performed to measure the number of localizations generated by a single Hb-AF647 molecule (calibration value). The number of Hb-AF647 proteins was then obtained by dividing the number of counted localization per bacterium by the calibration value. Despite this approach provides only an estimate of the number of proteins, it is straightforward and direct, and it proved to be effective for the measurement of overall surface densities of proteins on cancer cells [26, 28].

Here, two separate calibration experiments were carried out. In the first one, Hb-AF647 was deposited at very low concentrations (≤ 100 pM) on the glass coverslip to ensure that proteins are isolated and sparse. Each protein generated a small cluster of d-STORM localizations that was easily quantified with a clustering algorithm (Figure S3). In a second experiment, the same clustering algorithm was applied to images of the sample where Hb-AF647 was exposed to *S. aureus* grown in absence of DiP, assuming that most of the observed clusters were generated by single Hb-AF647 proteins. The two experiments gave comparable results, yielding a final calibration value of 5 localizations per Hb-AF647, in line with previous results [26, 28]. Using this calibration, the mean absolute number of Hb-AF647 molecules visible in the d-STORM images ranged from ~ 60, for *S. aureus* grown in absence of DiP, to ~ 360, for bacteria grown with 1 mM DiP (Figure 4). Importantly, control experiments performed using dye-conjugated myoglobin (Mb-AF647), instead of Hb-AF647, or exposing bacteria to Hb-AF647 and an excess of unlabeled Hb showed significantly lower protein counts, ensuring the specific detection of surface bound Hb-AF647 (Figure 4; Figure S1).

It should be noted that the number of Hb-AF647 counted from d-STORM images does not include all the proteins captured on the whole bacterial surface, but only those that are in proximity to the focal plane of the microscope. To estimate the actual surface density of Hb-AF647, we developed a simple geometric model that uses the ring-like pattern of the reference WGA-AF488 signal to obtain the extent of the bacterial surface which contributes to the observed d-STORM images (see Technical Notes with Figures S4 and S5). In this way, we estimated a mean surface density of ~ 240 Hb/μm^2 for *S.aureus* grown under Fe starving conditions (1 mM DiP, Figure 4), which gives ~ 450 Hb captured on the whole bacterial cell surface. The Hb density values reduced significantly for bacterial grown with lower concentrations of DiP, i.e., with higher Fe availability: ~ 160 Hb/μm^2 at 0.5 mM DiP, ~ 80 Hb/μm^2 at 0.25 mM DiP and 40 Hb/μm^2 in absence of DiP (Figure 4). These densities give, respectively, ~ 300, ~150, and ~80 Hb proteins on the whole bacterial surface.

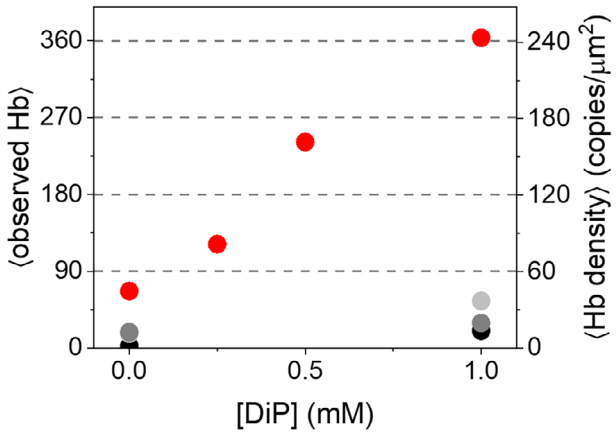


FIGURE 4 | Hb copies on single *S. aureus* cells. Mean number of observed Hb molecules per bacterium, visible in d-STORM images, as a function of the concentration of DiP in bacteria growth medium (red). The corresponding mean surface density of proteins is displayed on the right axis. The results obtained in control experiments performed exposing bacteria to 4 μM Hb-AF647 and 40 μM unlabeled Hb, either simultaneously (dark grey) or sequentially (light grey) are also shown, together with those obtained exposing bacteria to 4 μM Mb-AF647 (black), instead of Hb-AF647.

The values are affected by a relatively large uncertainty, due to the intrinsic cell-to-cell variability and to the approximations of the analysis model and should be regarded as estimates. Still, this approach provides an absolute quantification of the Hb copies on individual bacterial cells, and their changes in response to Fe availability. This is an advancement compared to more traditional imaging or bulk methods of protein quantification, e.g., gel electrophoresis techniques, flow cytometry or spectroscopy, which are limited to relative comparisons.

2.5 | A Hb-Based Photo-Antimicrobial Construct and its Loading on S. Aureus

The above results demonstrate that d-STORM can be exploited to quantify the extent of binding between Hb as physiological ligand and its Isd system receptors, at the single molecule and single cell level. Importantly, this quantitative analysis could find a direct application in the related context of antimicrobials

16136829, 0, Downloaded from https://onlinelibrary.wiley.com/doi/10.1002/smll.75276 by CochraneItalia, Wiley Online Library on [18/08/2026]. See the Terms and Conditions (https://onlinelibrary.wiley.com/terms-and-conditions) on Wiley Online Library for rules of use; OA articles are governed by the applicable Creative Commons License

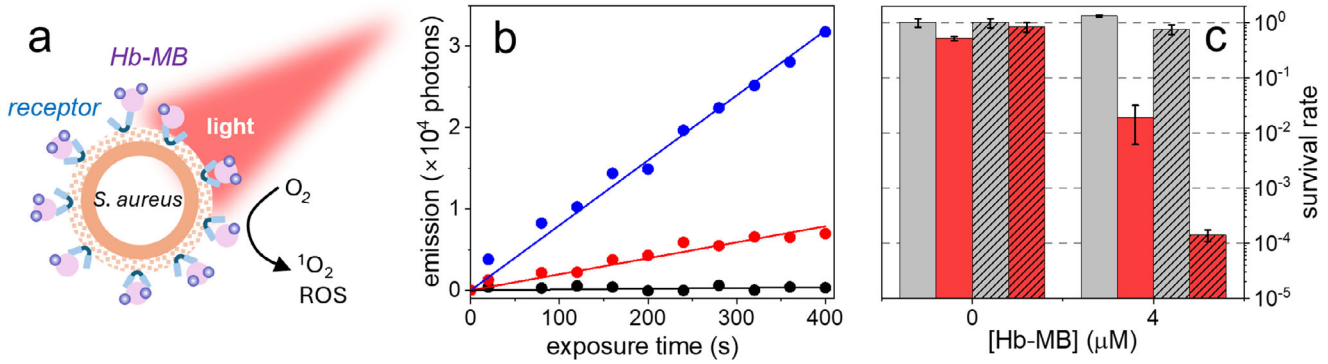


FIGURE 5 | A Hb-based photo-antimicrobial construct and its efficacy on *S. aureus*. (a) Schematic representation of the Hb-MB photosensitizing conjugate: the targeting moiety (Hb) binds to available receptors on *S. aureus* wall and, upon exposure to red light, the photosensitizing moiety (MB) reacts with molecular oxygen generating $^1O_2$ and other reactive oxygen species. (b) Fluorescence emission intensity at 528 nm of the singlet oxygen sensor green at increasing times of exposure to red light. The measurement was performed on solutions containing the sensor and either free MB (blue), as a reference, or Hb-MB (red). A control measurement on a solution containing only the sensor was also performed (black). The lines show the results of a fitting with a linear model. (c) *S. aureus* survival rate, obtained from colony forming units per mL, for bacteria incubated with 0 and 4 μM Hb-MB and exposed to red light (red) or kept in the dark (grey). The plain bars refer to measurements performed on bacteria grown in absence of DiP, the bars with stripes are for bacteria grown in the presence of 1 mM DiP. Fluence 222 J/cm^2 at 660±10 nm.

targeting the Isd system. The heme-acquisition machinery of *S. aureus* has previously been exploited for targeted photodynamic inactivation (PDI) using the photoactive fluorescent hemin analogue Ga (III)-protoporphyrin IX, either as a free photosensitizer or incorporated into Hb-based nanoparticle constructs [29, 30]. Building on this concept, Hb can serve directly both as a targeting agent and as a carrier for the delivery of photoactive molecules to the bacterial surface. From this perspective, the density of Hb molecules loaded on bacteria appears as a fundamental parameter, since a positive correlation is expected between the number of effective constructs bound to the target and treatment efficacy. In fact, a precise estimate of functional molecules density could foster a more rational development of treatments, by increasing their strength and reducing off-target effects in drug delivery.

As a proof of this concept, we developed a photoactive system by conjugating Hb with the small organic photosensitizing molecule Methylene Blue (MB), obtaining a functional Hb-MB conjugate for targeted antimicrobialPDI. Upon exposure to red light, MB molecules are photo-excited to their electronic triplet state which readily reacts with surrounding molecular oxygen (O_2) to generate cytotoxic reactive oxygen species, in particular superoxide anion and O_2 in its excited singlet state ($^1O_2$) [31, 32], leading to bacterial inactivation. PDI is effective also against antibiotic resistant strains [33]. As represented in Figure 5a, the Hb moiety acts as a targeting unit that specifically brings the conjugate Hb-MB to available receptors on the surface of *S. aureus*.

A photo-physical characterization of the Hb-MB construct allowed to test if MB retains its photosensitizing properties upon conjugation with Hb. With this aim, using nanosecond laser flash photolysis on air-equilibrated solutions, we monitored the kinetics of the recovery of the MB ground state after pulsed laser excitation in order to determine the lifetime of the molecule triplet state (τ_T; see Figure S6). For the reference (MB in PBS), the kinetics occurs with a lifetime τ_T = (1.8±0.1) μs, a value typical for the triplet of a photosensitizer in air equilibrated aqueous solution at room temperature. For MB conjugated to Hb the lifetime becomes τ_T = (3.0±0.1) μs, as expected for a triplet state only slightly shielded by the protein scaffold from O_2 dissolved in solution. A similar value had been observed for MB bound to streptavidin [34].

The evaluation of the triplet formation quantum yield (Φ_T) for Hb-MB is hindered by the competitive absorption of Hb that results in a small amplitude of the transient absorption signal. Upon correction for this filter effect (Equation 1 within Materials and Methods section), Φ_T provided a significant value, 0.21±0.05. Consistently, an appreciable photosensitization of $^1O_2$ by Hb-MB exposed to red light (quantum yield of $^1O_2$ formation, Φ_Δ) was measured spectroscopically by monitoring the fluorescence emission at 528 nm of a $^1O_2$ fluorescent sensor at increasing red light exposure (Figure 5b). Applying a comparative approach using free MB (Φ_Δ = 0.5 [32]) as a reference, Φ_Δ = 0.19±0.05 was obtained (Equation 2 within Materials and Methods section). The similar reduction of both Φ_T and Φ_Δ values for Hb-MB compared to free MB suggests a partial quenching mechanism, most likely due to the interaction with protein amino acids around the conjugation site, occurring when MB is bound. However, these results confirm that Hb-MB can act as a photosensitizing agent, despite with lower photosensitization yields compared to free MB.

Bacterial photo-inactivation assays were then performed. As reported in Figures 5c, S. *aureus* grown in absence of DiP, incubated with Hb-MB and then exposed to red light (λ = 660 ± 10 nm; 222 J/cm^2), showed a 2-log reduction of the survival rate, compared to bacteria kept in the dark. After the same treatment with Hb-MB and red light, *S. aureus* grown under Fe starving conditions (with 1 mM DiP), where d-STORM results demonstrate higher Hb-MB binding to *S. aureus*, remarkably showed a 4-log reduction of the survival rate, compared to dark conditions (Figure 5c). No reduction of survival rate after light exposure was observed for bacteria that were not treated with Hb-MB, both in absence and in presence of DiP in the culture medium. Photo-inactivation treatments were carried out on bac-

16136829, 0, Downloaded from https://onlinelibrary.wiley.com/doi/10.1002/smll.75276 by CochraneItalia, Wiley Online Library on [18/08/2026]. See the Terms and Conditions (https://onlinelibrary.wiley.com/terms-and-conditions) on Wiley Online Library for rules of use; OA articles are governed by the applicable Creative Commons License

teria in the stationary growth phase, to ensure consistency with the conditions used in d-STORM experiments. These results, even if obtained under a limited set of conditions, demonstrate that: (I) the Hb-MB conjugate can reduce the bacterial survival rate in response to light excitation in vitro; (II) the antimicrobial efficacy of the photo-activated Hb-MB conjugate strongly depends on the amount of Hb bound to *S. aureus*.

Importantly, the marked heterogeneity observed in Hb loading on single bacteria (Figure 3), especially under Fe starving conditions, means that, even if exposed to an excess of Hb-MB, a fraction of the bacteria might remain unaffected by the photo-treatment, due to the low number of surface-bound molecules. Finally, the clustered organization of Hb on the cell surface (Figures 1 and 3) might also play a role, since densely packed proteins might favor quenching processes thereby reducing the photosensitization efficacy.

3 | Concluding Remarks

Quantification of the density of cell surface receptors with high sensitivity is of central importance for the improvement and development of effective diagnostic and therapeutic routines. For that reason, single molecule localization microscopy has been employed with eukaryotic cells to provide an absolute quantification of the molecular densities of, for example, membrane proteins and glycans [35, 36], CD56 receptors [37], epidermal growth factor receptors [28]. On the contrary, very few quantitative studies were performed on bacteria. Carsten et al. have extensively shown in a recent review [38] how overcoming the visible light diffraction limit has offered relevant advantages in studying bacterial cell biology, as synthesis and assembly of peptidoglycan, DNA and RNA metabolism, macromolecular machines involved in protein secretion and DNA replication. In this context we report localization and quantification of human Hb copies decorating *S. aureus* wall at the single molecule level. Using d-STORM microscopy, we were able to determine the subcellular position and the copy number of Hb molecules on the *S. aureus* surface. We estimated that, under Fe starving conditions induced by treating cells with 1 mM DiP, ~ 450 Hb molecules are bound to each bacterium. This number reduces to ~ 80 in absence of DiP. Additionally, the spatial distribution of Hb molecules on the single cell was highly discontinuous. This might reflect an intrinsic clustering of cell wall-anchored receptor proteins, but it may also arise from an irregular efficacy in the binding of Hb, e.g., due to steric hindrance or to variable affinity. As in this study bacteria are in their stationary growth phase when exposed to Hb, it is unclear whether the discontinuity can be explained with an accumulation of proteins at the cell division site. Moreover, the presence of two receptors for Hb binding, namely IsdB and IsdH, might be an additional source of heterogeneity. While further studies are needed to systematically investigate the origin of such heterogeneity in Hb capturing, we highlight how quantitative microscopy is a powerful tool to address these questions. Indeed, this methodology is not strictly limited to the localization and counting of Hb molecules but is broadly applicable to other relevant targets on the cell surface.

Furthermore, since binding of Hb is the primary step in the Fe acquisition process mediated by the Isd system, this quantification is expected to support the design of antimicrobial strategies alternative to more traditional antibiotics. To explore this concept, we then developed a photoactive derivative of Hb, by conjugating the protein to MB, and found that the photoinactivation efficiency is positively correlated with the number of Hb molecules bound, hence to the expression level of accessible Hb receptors. Even if limited to the model Hb-MB conjugate, these observations exemplify how single-molecule imaging can support a more precise evaluation of the action of targeted photo-antimicrobials, toward a more rational design of functional constructs.

4 | Experimental Section

4.1 | Materials

Human hemoglobin and equine heart myoglobin were from Sigma-Aldrich, WGA-AF488 and AF647 NHS ester were from Invitrogen. DiP (2,2'-bipyridyl) was from Sigma-Aldrich. Methylene Blue NHS ester was from Atto-tech GmbH.

Concentrations were estimated from the molar extinction coefficients of the compounds: ε (414 nm) = 524,280 $M^{-1}cm^{-1}$ for Hb, ε (409 nm) = 157,000 $M^{-1}cm^{-1}$ for myoglobin, ε (658 nm) = 270,000 $M^{-1}cm^{-1}$ for AF647 NHS ester, ε (663 nm) = 85,000 $M^{-1}cm^{-1}$ for (monomeric) methylene blue. The Hb concentration in Hb-AF647 complex was estimated from the absorbance at 414 nm after correcting for the AF647 contribution at this wavelength.

4.2 | AlexaFluor647- and MB-Protein Conjugates Preparation

The conjugates between the fluorophore (AF647 NHS ester) or the photosensitizer (MB NHS ester) and a hemoprotein (hemoglobin/myoglobin) were prepared using the same standard protocol. A concentrated stock of dye in DMSO was diluted in PBS buffer (pH 7.4) with 10% of $NaHCO_3$ (pH 8.5), and vortexed for 2 h at room temperature in dark. Then the conjugate was purified using a Sephadex G25, PD-10 column (Cytiva, Marlborough, MA, USA) equilibrated with PBS buffer at pH = 7.4.

The degree of labeling (DOL, which indicates the average number of dye molecules bound to each protein) was determined spectroscopically using a Jasco V650 spectrophotometer (Jasco Europe S.R.L., Milano, Italy). The obtained DOL, expressed as [fluorophore]/[protein] molar ratio, was of 1.6 dye molecules per protein for Hb-AF647 and 1.1 for Hb-MB.

4.3 | Photophysical Properties of the Conjugate for Bacteria Photo-Inactivation

The relaxation of the triplet state of MB conjugated to Hb has been monitored at 633 nm upon excitation with the second harmonic at 532 nm of a pulsed Nd:Yag laser (Surelite I-10, Continuum, San Jose, CA, USA), using a set up previously described [39, 40, 41]. The quantum yield of triplet formation was estimated using

16136829, 0, Downloaded from https://onlinelibrary.wiley.com/doi/10.1002/smll.75276 by CochraneItalia, Wiley Online Library on [18/08/2026]. See the Terms and Conditions (https://onlinelibrary.wiley.com/terms-and-conditions) on Wiley Online Library for rules of use; OA articles are governed by the applicable Creative Commons License

a comparative method, defined by the equation:

$$\Phi_{T,X} = \Phi_{T,R} \left(\frac{\Delta A_X}{\Delta A_R}\right) \left(\frac{1-10^{-A_R}}{1-10^{-A_X}}\right) \left(\frac{A_{Hb-MB}}{A_X}\right) \quad (1)$$

where $\Phi_{T,R}$ and $\Phi_{T,X}$ are triplet quantum yield of MB in PBS (reference compound) and Hb-MB complex, respectively, A_R, A_X and $A_{Hb\text{-}MB}$ the absorbance values at 532 nm of the reference, of MB in the complex and of the complex, ΔA_R and ΔA_X the values obtained from the measured transient absorbance changes. MB in PBS was considered as a reference compound (0.52 [32]) and the kinetics was followed at 633 nm, where bleaching of the ground state is observed. The last factor in Equation 1 has been introduced as a correction for the filter effect due to Hb absorption at 532 nm in the complex.

A comparative method was exploited to evaluate the singlet oxygen ($^1O_2$) quantum yield when MB is conjugated to Hb using MB in PBS as a reference and singlet oxygen sensor green (SOSG) (Invitrogen). The procedure is based on the linear relationship between SOGS fluorescence emission and the photo-induced $^1O_2$ concentration. SOSG was dissolved in methanol to obtain a 5 mM stock solution, that was diluted in PBS solutions containing MB and Hb-MB. The sample (Hb-MB), the reference (MB in PBS) and a control solution containing only SOGS were progressively illuminated using a cw He:Ne laser (Melles Griot, 30 mW at 633 nm). SOSG fluorescence emission was measured (λ_{ex} = 488 nm) after progressive illumination steps of 20 s, repeated up to a total of 160 s. A linear fitting can be used to analyze the emission intensity increase and the slopes of the sample and the reference, upon correction for SOGS contribution, permit to calculate the singlet oxygen quantum yield according to the equation:

$$\Phi_{\Delta,X} = \Phi_{\Delta,R} \left(\frac{slope_X}{slope_R}\right) \left(\frac{1-10^{-A_R},633}{1-10^{-A_{X,633}}}\right) \left(\frac{1-10^{-A_{SOSG,R,488}}}{1-10^{-A_{SOSG,X,488}}}\right) \left(\frac{A_{X,488}}{A_{R,488}}\right) \quad (2)$$

where:

$\Phi_{\Delta,R}$ and $\Phi_{\Delta,X}$ are $^1O_2$ quantum yield of the reference (MB in PBS, 0.5 [32, 34]) and Hb-MB, respectively, $A_{R,633}$ and $A_{X,633}$ the absorbance values of the photosensitizer at 633 nm $A_{SOSG,R,488}$ and $A_{SOSG,X,488}$ the absorbance values of SOSG at 488 nm in reference and sample solution respectively, $slope_R$ and $slope_X$ the values retrieved from the linear fitting. The last factor in Equation 2 has been introduced as a correction for the filter effect due to Hb absorption at 488 nm in the complex.

4.4 | Bacteria Preparation for Imaging

A colony of *S. aureus* ATCC25923 was picked from blood agar plate and inoculated in 3 mL of TSB medium with different DiP concentrations (0, 0.25, 0.5, and 1 mM). The inoculum was incubated at 37°C, 180 rpm, for 22 h to reach the stationary phase of growth (OD_{600}>1).

For each culture condition, 300 µl of the stationary phase culture were pelleted at 3000 g for 5 min, washed once in PBS, then, incubated with 100 µl of the Hb-AF647 conjugate (final concentration 4 µM) for 1 h, followed by fixation with PFA 2% for 10 min. Fixed bacteria were blocked in glycine 300 mM for 20 min, then in BSA 30 mg/mL for 20 min. Finally, bacterial cells were pelleted and resuspended at an OD_{600} of approximately 0.3 in PBS.

The bacteria were then placed in Lab-Tek chambers (pre-treated with poly-L-lysine 0.1 mg/mL for 20 min at room temperature) and allowed to adhere for 20 min. After a PBS wash, bacteria were incubated with WGA-Alexa488 (25 nM) for 10 min at room temperature. Before d-STORM imaging, a STORM buffer composed of PBS with cysteamine (100 mM), glucose (5% w/v), glucose oxidase (0.5 mg/mL) and catalase (40 µg/mL) was introduced. All the procedures were carried out at room temperature in the dark.

4.5 | Instrumentation. d-STORM Imaging

d-STORM images were acquired with an Oxford Nanoimaging (ONI) Nanoimager-S Mark III microscope equipped with four excitation lasers (405, 488, 561, and 640 nm) and a 100×/NA1.4 oil immersion objective (Olympus, Tokyo, Japan). The fluorescence emission was collected by the objective, split into two spectrally separated channels (576–620 nm and 665–705 nm) by a 640LP dichroic beam-splitter, and recorded using a CMOS camera (Hamamatsu OrcaFlash 4.0) to obtain 428 × 684 images with a pixel size of 117 nm. All measurements were performed at 28°C and using HILO (highly inclined and laminated optical sheet) configuration which improves signal-to-noise ratio and enables precise focusing of bacterial cells.

Samples were acquired for 10000 frames using continuous 640 nm (322 mW) excitation, followed by 20000 frames using continuous 488 nm (245 mW) and 405 nm (0.1 mW) excitation. The camera exposure time was 10 ms per frame. The acquired frames were processed with the NimOS software 1.19.4 from ONI. In each frame, a single emitting fluorophore was fitted with a 2D Gaussian model to determine the center position of the localization. The localizations obtained were brought together to reconstruct the final d-STORM image. Localizations that were too weak (below 1000 detected photons in the green channel and below 700 detected photons in the red channel) or acquired during initial equilibration (first 500 acquisition frames for the 640 nm excitation and between 10000–12000 frames for the 488 nm excitation) were discarded. Prior to imaging measurements, an alignment of the two spectrally separated acquisition channels was performed using TetraSpeck microspheres (0.1 µm, Invitrogen) by means of a specific tool of the NimOS software. This avoids systematic shifts between the two colors in the d-STORM images. Effect of residual mechanical drift of the sample occurring during acquisition was negligible but it was anyway corrected by a redundant autocorrelation algorithm of the NimOS software.

4.6 | Instrumentation. Fluorescence Correlation Spectroscopy

Fluorescence correlation spectroscopy (FCS) experiments were carried out using a Microtime 200 system from PicoQuant,

16136829, 0, Downloaded from https://onlinelibrary.wiley.com/doi/10.1002/smll.75276 by CochraneItalia, Wiley Online Library on [18/08/2026]. See the Terms and Conditions (https://onlinelibrary.wiley.com/terms-and-conditions) on Wiley Online Library for rules of use; OA articles are governed by the applicable Creative Commons License

based on an inverted confocal microscope (Olympus IX71) and equipped with two SPADs (Single Photon Avalanche Diodes). The cross-correlation mode was exploited in all experiments. AF647 excitation was achieved by a 635 nm picosecond diode laser operated at 20 MHz. Fluorescence emission was collected through a bandpass filter (675/25 nm) and split with a 50/50 splitter between the two detection channels. Photon binning is 1 ms.

A *S. aureus* suspension (grown in TSB enriched with 0.25 mM DiP) was washed with PBS to remove the culture medium from the aqueous solution. Then, bacteria (OD_{600} = 0.3) were incubated with Hb-AF647 (1 nM) for 1 h at room temperature.

4.7 | Photoinactivation of *S. aureus* Suspensions

A colony of *S. aureus* ATCC25923 was picked from blood agar plate and inoculated in 3 mL of TSB medium with different DiP concentrations (0, and 1 mM; from a 10 mM stock solution in water). The inoculum was left to incubate at 37°C, 180 rpm, for 22 h to reach the stationary phase. After that, the culture reaches an OD of at least 1.3 (slightly higher without DiP, ~1.5), indicating entry into the stationary phase.

After the growth, the bacteria solution was washed twice by centrifugation (3000 g for 5 min) and diluted to an OD_{600} = 0.2, corresponding to an initial concentration of bacteria of 10^6 Colony forming units/mL (CFU/mL). Then, the bacteria were incubated with the Hb-MB complex (4 μM) for 1 h at room temperature in the dark. Suspensions (200 μL) were placed in 96-well plates and illuminated from the top with red light for 70 min using a LED light source (Red Light Man lamp) with power of 53 mW/cm^2 at 660±10 nm.

Suspensions were then serially diluted until 10–^{6} times the original concentration and 10 μL of the diluted suspensions were plated on tryptic soy agar plates. Experiments were carried out in duplicate for each condition, including cell and dark controls. CFUs were counted, after 24 h incubation in the dark at 37°C, to calculate the survival fraction.

Acknowledgements

S.A. acknowledges support from University of Parma "Bando di Ateneo per la Ricerca 2024 – Azione A". C.V. acknowledges EU funding within the NextGenerationEU-MUR PNRR Extended Partnership initiative on Emerging Infectious Diseases (Project no. PE00000007, INF-ACT). INF-ACT Cascade Open Call 2023 (COC-1- 2023-CNR). The cost of the d-STORM microscope used for this experimental investigation was supported by the Italian Ministry of Universities and Research (D.M. n. 737-25/06/2021) and cofunded by the University of Parma through the "Scientific Instrumentation Upgrade Programme 2021". This work was also supported by funds from the Spanish Ministerio de Ciencia e Innovación-Agencia Estatal de Investigación (MCI/AEI/10.13039/501100011033) and FEDER (Project PID2023-149483NB-C22). S.N. thanks the Departament de Recerca i Universitats de la Generalitat de Catalunya for the support given to our research group (2021 SGR 01023) and the ICREA-Catalan Institution for Research and Advanced Studies for Grant Number. Ac2232308.

Open access publishing facilitated by Universita degli Studi di Parma, as part of the Wiley - CRUI-CARE agreement.

Conflicts of Interest

The authors declare no conflict of interest.

Data Availability Statement

The data that support the findings of this study are available from the corresponding author upon reasonable request.

References

1. T. J. Foster, "Antibiotic resistance in Staphylococcus aureus. Current status and future prospects," *FEMS Microbiology Reviews* 41, no. 3 (2017): 430–449, https://doi.org/10.1093/femsre/fux007.

2. K. Kavanagh, "The Rise of 'Nightmare Bacteria': Antimicrobial Resistance in Five Charts," *Nature* 646, no. 8085 (2025): 526–527, https://doi.org/10.1038/d41586-025-03218-x.

3. M. Caza and J. W. Kronstad, "Shared and Distinct Mechanisms of Iron Acquisition by Bacterial and Fungal Pathogens of Humans," *Frontiers in Cellular and Infection Microbiology* 3 (2013): 3, https://doi.org/10.3389/fcimb.2013.00080.

4. N. D. Hammer and E. P. Skaar, "Molecular Mechanisms of *Staphylococcus Aureus* Iron Acquisition," *Annual Review of Microbiology* 65, no. 1 (2011): 129–147, https://doi.org/10.1146/annurev-micro-090110-102851.

5. S. K. Mazmanian, E. P. Skaar, A. H. Gaspar, et al., "Passage of Heme-Iron Across the Envelope of *Staphylococcus Aureus*," *Science* 299, no. 5608 (2003): 906–909, https://doi.org/10.1126/science.1081147.

6. E. P. Skaar, M. Humayun, T. Bae, K. L. DeBord, and O. Schneewind, "Iron-Source Preference of *Staphylococcus Aureus* Infections," *Science* 305, no. 5690 (2004): 1626–1628, https://doi.org/10.1126/science.1099930.

7. G. Pishchany, J. R. Sheldon, C. F. Dickson, et al., "IsdB-Dependent Hemoglobin Binding Is Required for Acquisition of Heme by Staphylococcus Aureus," *The Journal of Infectious Diseases* 209, no. 11 (2014): 1764–1772, https://doi.org/10.1093/infdis/jit817.

8. L. Visai, N. Yanagisawa, E. Josefsson, et al., "Immune Evasion by Staphylococcus Aureus Conferred by Iron-Regulated Surface Determinant Protein IsdH," *Microbiology* 155, no. 3 (2009): 667–679, https://doi.org/10.1099/mic.0.025684-0.

9. V. B. Comani, O. De Bei, G. Paris, et al., "Refining the Mechanism of Heme Acquisition From Free Hemoglobin by Staphylococcus Aureus IsdH," *Proceedings of the National Academy of Sciences* 123, no. 20 (2026): 2601134123, https://doi.org/10.1073/pnas.2601134123.

10. M. Cozzi, M. Failla, E. Gianquinto, et al., "Identification of Small Molecules Affecting the Interaction Between Human Hemoglobin and Staphylococcus Aureus IsdB Hemophore," *Scientific Reports* 14, no. 1 (2024): 8272, https://doi.org/10.1038/s41598-024-55931-8.

11. H. K. Kim, A. DeDent, A. G. Cheng, et al., "IsdA and IsdB Antibodies Protect Mice Against Staphylococcus Aureus Abscess Formation and Lethal Challenge," *Vaccine* 28, no. 38 (2010): 6382–6392, https://doi.org/10.1016/j.vaccine.2010.02.097.

12. M. R. Bennett, R. G. Bombardi, N. Kose, et al., "Human mAbs to Staphylococcus Aureus IsdA Provide Protection Through Both Heme-Blocking and Fc-Mediated Mechanisms," *The Journal of Infectious Diseases* 219, no. 8 (2019): 1264–1273, https://doi.org/10.1093/infdis/jiy635.

13. S. Valenciano-Bellido, J. M. M. Caaveiro, M. Nakakido, et al., "Targeting Hemoglobin Receptors IsdH and IsdB of Staphylococcus Aureus With a Single VHH Antibody Inhibits Bacterial Growth," *Journal of Biological Chemistry* 299, no. 9 (2023): 104927, https://doi.org/10.1016/j.jbc.2023.104927.

14. S. L. Drury, A. R. Miller, C. L. Laut, et al., "Simultaneous Exposure to Intracellular and Extracellular Photosensitizers for the Treatment of

16136829, 0, Downloaded from https://onlinelibrary.wiley.com/doi/10.1002/smll.75276 by Cochraneltalia, Wiley Online Library on [18/08/2026]. See the Terms and Conditions (https://onlinelibrary.wiley.com/terms-and-conditions) on Wiley Online Library for rules of use; OA articles are governed by the applicable Creative Commons License

Staphylococcus Aureus Infections," *Antimicrobial Agents and Chemotherapy* 65, no. 12 (2021): e0091921.

15. B. A. Fonner, B. P. Tripet, B. J. Eilers, et al., "Solution Structure and Molecular Determinants of Hemoglobin Binding of the First NEAT Domain of IsdB in *Staphylococcus Aureus*," *Biochemistry* 53, no. 24 (2014): 3922–3933, https://doi.org/10.1021/bi5005188.

16. O. De Bei, M. Marchetti, L. Ronda, et al., "Cryo-EM Structures of Staphylococcal IsdB Bound to Human Hemoglobin Reveal the Process of Heme Extraction," *Proceedings of the National Academy of Sciences* 119, no. 14 (2022): 2116708119, https://doi.org/10.1073/pnas.2116708119.

17. O. De Bei, M. Marchetti, S. Guglielmo, et al., "Time-Resolved X-Ray Solution Scattering Unveils the Events Leading to Hemoglobin Heme Capture by Staphylococcal IsdB," *Nature Communications* 16, no. 1 (2025): 1361, https://doi.org/10.1038/s41467-024-54949-w.

18. G. Pishchany, S. E. Dickey, and E. P. Skaar, "Subcellular Localization of the *Staphylococcus Aureus* Heme Iron Transport Components IsdA and IsdB," *Infection and Immunity* 77, no. 7 (2009): 2624–2634, https://doi.org/10.1128/IAI.01531-08.

19. S. Van De Linde, A. Löschberger, T. Klein, et al., "Direct Stochastic Optical Reconstruction Microscopy With Standard Fluorescent Probes," *Nature Protocols* 6, no. 7 (2011): 991–1009, https://doi.org/10.1038/nprot.2011.336.

20. D. H. Atha and A. Riggs, "Tetramer-Dimer Dissociation in Homoglobin and the Bohr Effect," *Journal of Biological Chemistry* 251, no. 18 (1976): 5537–5543, https://doi.org/10.1016/S0021-9258(17)33093-4.

21. L. R. Manning, W. T. Jenkins, J. R. Hess, K. Vandegriff, R. M. Winslow, and J. M. Manning, "Subunit Dissociations in Natural and Recombinant Hemoglobins," *Protein Science* 5, no. 4 (1996): 775–781, https://doi.org/10.1002/pro.5560050423.

22. Y.-X. Huang, Z.-J. Wu, B.-T. Huang, and M. Luo, "Pathway and Mechanism of pH Dependent Human Hemoglobin Tetramer-Dimer-Monomer Dissociations," *PLoS ONE* 8, no. 11 (2013): 81708, https://doi.org/10.1371/journal.pone.0081708.

23. D. Pezzuoli, M. Cozzolino, C. Montali, et al., "Serum Albumins Are Efficient Delivery Systems for the Photosensitizer Hypericin in Photosensitization-Based Treatments Against Staphylococcus Aureus," *Food Control* 94 (2018): 254–262, https://doi.org/10.1016/j.foodcont.2018.07.027.

24. J. M. Monteiro, P. B. Fernandes, F. Vaz, et al., "Cell shape dynamics During the staphylococcal cell cycle," *Nature Communications* 6, no. 1 (2015): 8055, https://doi.org/10.1038/ncomms9055.

25. T. Nerreter, S. Letschert, R. Götz, et al., "Super-Resolution Microscopy Reveals Ultra-Low CD19 Expression on Myeloma Cells That Triggers Elimination by CD19 CAR-T," *Nature Communications* 10, no. 1 (2019): 3137, https://doi.org/10.1038/s41467-019-10948-w.

26. P. Delcanale, M. M. Alampi, A. Mussini, et al., "A Photoactive Supramolecular Complex Targeting PD-L1 Reveals a Weak Correlation Between Photoactivation Efficiency and Receptor Expression Levels in Non-Small-Cell Lung Cancer Tumor Models," *Pharmaceutics* 15, no. 12 (2023): 2776, https://doi.org/10.3390/pharmaceutics15122776.

27. S. Hugelier, P. L. Colosi, and M. Lakadamyali, "Quantitative Single-Molecule Localization Microscopy," *Annual Review of Biophysics* 52, no. 1 (2023): 139–160, https://doi.org/10.1146/annurev-biophys-111622-091212.

28. L. Woythe, P. Madhikar, N. Feiner-Gracia, C. Storm, and L. Albertazzi, "A Single-Molecule View at Nanoparticle Targeting Selectivity: Correlating Ligand Functionality and Cell Receptor Density," *ACS Nano* 16, no. 3 (2022): 3785–3796, https://doi.org/10.1021/acsnano.1c08277.

29. A. V. Morales-de-Echegaray, T. R. Maltais, L. Lin, et al., "Rapid Uptake and Photodynamic Inactivation of Staphylococci by Ga(III)-Protoporphyrin IX," *ACS Infectious Diseases* 4, no. 11 (2018): 1564–1573, https://doi.org/10.1021/acsinfecdis.8b00125.

30. A. V. Morales-de-Echegaray, L. Lin, B. Sivasubramaniam, et al., "Antimicrobial Photodynamic Activity of Gallium-Substituted Haemoglobin on Silver Nanoparticles," *Nanoscale* 12, no. 42 (2020): 21734–21742, https://doi.org/10.1039/C9NR09064A.

31. P. R. Ogilby, "Singlet Oxygen: There Is Indeed Something New Under the Sun," *Chemical Society Reviews* 39, no. 8 (2010): 3181, https://doi.org/10.1039/b926014p.

32. J. P. Tardivo, A. Del Giglio, C. S. De Oliveira, et al., "Methylene Blue in Photodynamic Therapy: From Basic Mechanisms to Clinical Applications," *Photodiagnosis and Photodynamic Therapy* 2, no. 3 (2005): 175–191, https://doi.org/10.1016/S1572-1000(05)00097-9.

33. P. Delcanale, S. Abbruzzetti, and C. Viappiani, "Photodynamic Treatment of Pathogens," *La Rivista del Nuovo Cimento* 45, no. 6 (2022): 407–459, https://doi.org/10.1007/s40766-022-00031-4.

34. A. Mussini, P. Delcanale, M. Berni, et al., *IJMS* 25, no. 11 (2024): 5751, https://doi.org/10.3390/ijms25115751.

35. P. Mateos-Gil, S. Letschert, S. Doose, and M. Sauer, "Super-Resolution Imaging of Plasma Membrane Proteins With Click Chemistry," *Frontiers in Cell and Developmental Biology* 4 (2016): 4, https://doi.org/10.3389/fcell.2016.00098.

36. L. A. Masullo, K. Almahayni, I. Pachmayr, et al., "Ångström-Resolution Imaging of Cell-Surface Glycans," *Nature Nanotechnology* 20, no. 10 (2025): 1457–1463, https://doi.org/10.1038/s41565-025-01966-5.

37. F. Wäldchen, J. Schlegel, R. Götz, et al., "Whole-Cell Imaging of Plasma Membrane Receptors by 3D Lattice Light-Sheet dSTORM," *Nature Communications* 11, no. 1 (2020): 887, https://doi.org/10.1038/s41467-020-14731-0.

38. A. Carsten, M. Wolters, and M. Aepfelbacher, "Super-resolution fluorescence microscopy for investigating bacterial cell biology," *Molecular Microbiology* 121, no. 4 (2024): 646–658, https://doi.org/10.1111/mmi.15203.

39. S. Abbruzzetti, S. Bruno, S. Faggiano, E. Grandi, A. Mozzarelli, and C. Viappiani, "Time-Resolved Methods in Biophysics. 2. Monitoring Haem Proteins at Work With Nanosecond Laser Flash Photolysis," *Photochemical & Photobiological Sciences* 5, no. 12 (2006): 1109–1120, https://doi.org/10.1039/b610236k.

40. S. Abbruzzetti, S. Sottini, C. Viappiani, and J. E. T. Corrie, "Acid-Induced Unfolding of Myoglobin Triggered by a Laser pH Jump Method," *Photochemical & Photobiological Sciences* 5, no. 6 (2006): 621–628, https://doi.org/10.1039/b516533d.

41. S. Bruno, S. Faggiano, F. Spyrakis, et al., "Different Roles of Protein Dynamics and Ligand Migration in Non-Symbiotic Hemoglobins AHb1 and AHb2 From Arabidopsis Thaliana," *Gene* 398, no. 1–2 (2007): 224–233, https://doi.org/10.1016/j.gene.2007.02.042.

Supporting Information

Additional supporting information can be found online in the Supporting Information section.

Supporting file: smll75276-sup-0001-SuppMat.docx

16136829, 0, Downloaded from https://onlinelibrary.wiley.com/doi/10.1002/smll.75276 by CochraneItalia, Wiley Online Library on [18/08/2026]. See the Terms and Conditions (https://onlinelibrary.wiley.com/terms-and-conditions) on Wiley Online Library for rules of use; OA articles are governed by the applicable Creative Commons License